Correlations between oxygen octahedral distortions and magnetic and transport properties in strained $La_{0.5}Sr_{0.5}CoO_3$ thin films

Yooun Heo,[1] Daisuke Kan,[1,*] Masato Anada,[2] Yusuke Wakabayashi,[2,†] Hiroo Tajiri,[3] and Yuichi Shimakawa[1,4]

[1]*Institute for Chemical Research, Kyoto University, Uji, Kyoto 611-0011, Japan*

[2]*Division of Materials Physics, Graduate School of Engineering Science, Osaka University, Toyonaka, Osaka 560–8531, Japan*

[3]*Japan Synchrotron Radiation Research Institute, SPring-8, Sayo, Hyogo 679–5198, Japan*

[4]*Integrated Research Consortium on Chemical Sciences, Uji, Kyoto 611-0011, Japan*

(Received 21 February 2019; revised manuscript received 11 April 2019; published 21 May 2019)

We quantitatively evaluated oxygen octahedral distortions in epitaxial thin films of the itinerant ferromagnet, $La_{0.5}Sr_{0.5}CoO_3$ (LSCO), and investigated their impact on strucure-property relationships. The compressively strained film on a $LaAlO_3$ substrate has a lower electrical resistivity and higher ferromagnetic transition temperature than the tensilely strained film on a $La_{0.30}Sr_{0.70}Al_{0.65}Ta_{0.35}O_3$ substrate. The magnetic anisotropy is also found to depend on the type of strain, with perpendicular magnetic anisotropy induced in the compressively strained film and in-plane magnetization seen in the tensilely strained film. Our synchrotron x-ray-diffraction measurements and quantitative analysis reveal distinct oxygen octahedral distortions accommodated in these films and show that the out-of-plane and in-plane Co–O bond lengths of the compressively strained film are comparable to the in-plane and out-of-plane bond lengths of the tensilely strained film. These results indicate that the bond-length changes in LSCO modify hybridization between Co 3*d* and *O2p* orbitals, leading to the strain-dependent properties. These results highlight the significant role of octahedral distortions for structure-property relationships in the strained LSCO films.

DOI: 10.1103/PhysRevB.99.174420

I. INTRODUCTION

A variety of functional properties seen in transition metal oxides are closely linked with their structural distortions characterized by either cation displacements or oxygen coordination environments. Heterostructuring oxides having different structural distortions by employing advanced thin-film epitaxy techniques has been shown to introduce and stabilize distortions not seen in bulk materials, allowing one to engineer and explore functional properties such as (multi-) ferroelectricity and magnetism [1–7]. However, structural distortions accommodated in heterostructured oxides vary in rather complex manners because they strongly depend on structural mismatches between constituent materials [8–13]. Therefore, understanding how structural distortions are accommodated in oxide heterostructures and how the distortions are linked to physical properties are important.

Bulk $La_{0.5}Sr_{0.5}CoO_3$ (LSCO) is an itinerant ferromagnet and has the *R*-3*c* rhombohedral perovskite structure with pseudocubic subcell ($a_{pc} \sim 3.84$ Å and $\alpha_{pc} \sim 90.2°$) at room temperature. The CoO_6 octahedra are rotated in the pattern of $a^-a^-a^-$ in Glazer notation [14], and the rotation angle α_{rot} is ∼1.6° [15–17]. This oxide becomes a ferromagnet below ∼230 K [18]. Previously it was found that the epitaxial thin films of LSCO and other perovskite cobaltites exhibit modified magnetic properties from those of the bulk materials [19–23], implying that CoO_6 oxygen octahedral distortions in the films differ from those in the bulk materials and impact the films' structure-property relationships. However, quantitatively evaluating octahedral distortions requires precise determinations of atomic positions of both cations and oxygens, which are experimentally difficult [24–26]. How octahedral distortions are accommodated in LSCO epitaxial thin films and how they impact films' structure-property relationships remains elusive.

In this study, we fabricated by pulsed-laser deposition (PLD) compressively and tensilely strained LSCO thin films on $LaAlO_3$ (LAO) and $La_{0.30}Sr_{0.70}Al_{0.65}Ta_{0.35}O_3$ (LSAT) substrates, respectively, and investigated CoO_6 octahedral distortions accommodated in the epitaxial thin films and their link to magnetic and transport properties. Our structural and magnetotransport characterizations show that the compressively strained film on the LAO substrate has a lower electrical resistivity and higher ferromagnetic transition temperature than the tensilely strained film on the LSAT substrate. The magnetic easy-axis directions are also found to be strain dependent. Based on our experimental results including synchrotron x-ray-diffraction measurements, CoO_6 octahedral distortions accommodated in the compressively and tensilely strained films and their influence on the films' strain-dependent properties are discussed.

II. EXPERIMENTAL DETAILS

Epitaxial LSCO thin films with a thickness of 10–15 nm were grown on as-supplied (001) LAO and (001) LSAT substrates (SHINKOSHA Co. Ltd.) by PLD. Due to the lattice mismatch between the LSCO and the substrates, LAO and

*dkan@scl.kyoto-u.ac.jp

†Present address: Department of Physics, Graduate School of Science, Tohoku University, Sendai 980–8578, Japan.

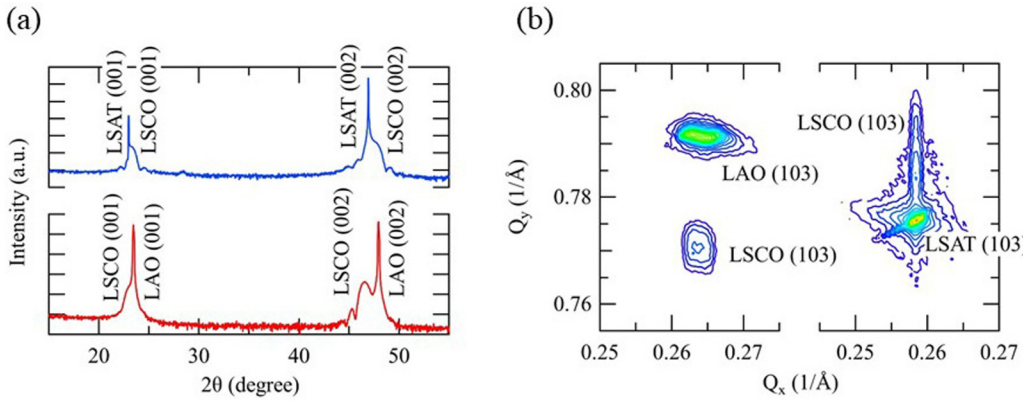

FIG. 1. X-ray-diffraction characterizations of LSCO films on LAO and LSAT substrates. (a) 2θ-θ profiles of LSCO films on LSAT (blue) and LAO (red) substrates. (b) Reciprocal space mappings around the (103) LAO (left) and LSAT (right) Bragg reflection for the LSCO films.

LSAT provide 1.2% compressive and 0.9% tensile strain to the film layer. During the film deposition, the stoichiometric LSCO pellet was ablated at 2 Hz with a KrF excimer laser ($\lambda = 248$ nm) with a laser spot density of 1 J/cm^2. Typical growth rate was $\sim$0.4 Å/s. The deposition of the LSCO layer was carried out at the substrate temperature of 600 °C and under the oxygen partial pressure of 100 mTorr (only oxygen and no additional gas were added). After deposition the films were cooled to room temperature under 100-mTorr oxygen pressure.

III. RESULTS AND DISCUSSION

Laboratory-source x-ray $2\theta/\theta$ profiles in Fig. 1(a) confirm the (001)-oriented epitaxial growth of the LSCO layer without any secondary phases. The out-of-plane lattice constants of the films on the LAO and LSAT substrates are, respectively, larger and smaller than those of bulk LSCO. Furthermore, the reciprocal space mappings around the (103) reflections of the substrates [Fig. 1(b)] show that the (103) LSCO reflections appear in the same position along the horizontal axis (the in-plane direction) as those for the substrates and that the in-plane lattice constants of the films are fixed by the substrates' lattices. These observations indicate that the substrate-induced compressive and tensile strain are imposed on the films on the LAO and LSAT substrates, respectively.

Figure 2 shows temperature dependence of the electrical resistivity ρ_{xx} and the magnetic moment M for the LSCO films under compressive and tensile strains (on the LAO and LSAT substrates, respectively). The ρ_{xx} was measured by the van der

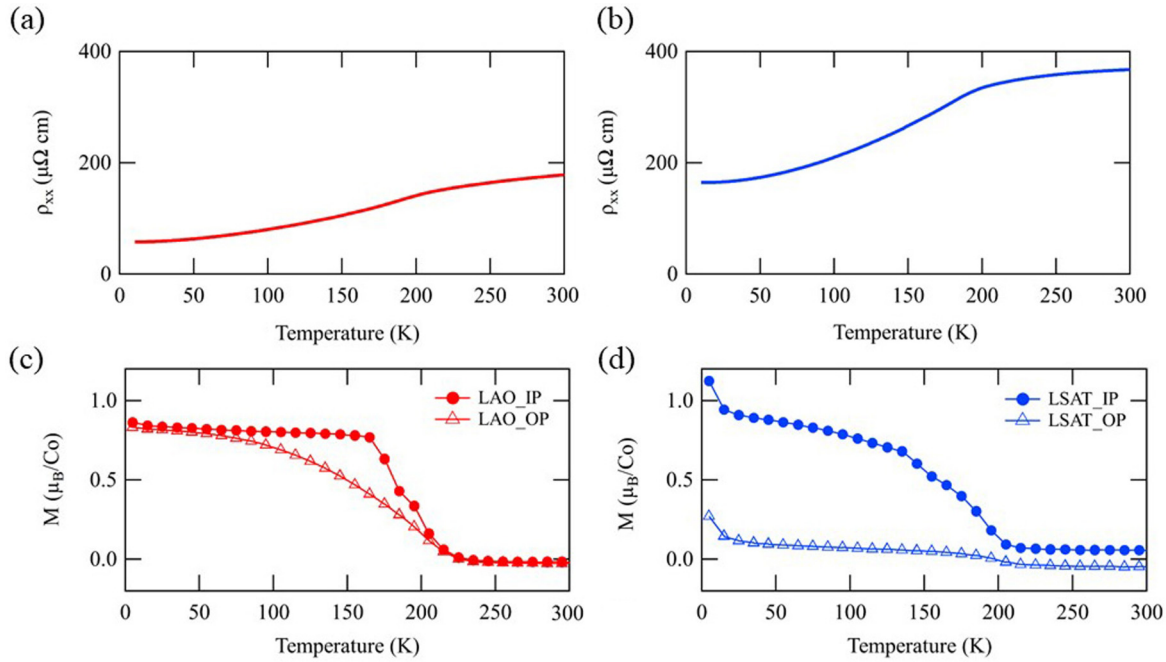

FIG. 2. Temperature dependence of the longitudinal resistivity ρ_{xx} (top) and magnetization M (bottom) of the LSCO films on (a), (c) LAO and (b) (d) LSAT substrates. For magnetization measurements, a magnetic field of 1000 Oe was applied in parallel and perpendicular directions to the film surface during the cooling process and measurement.

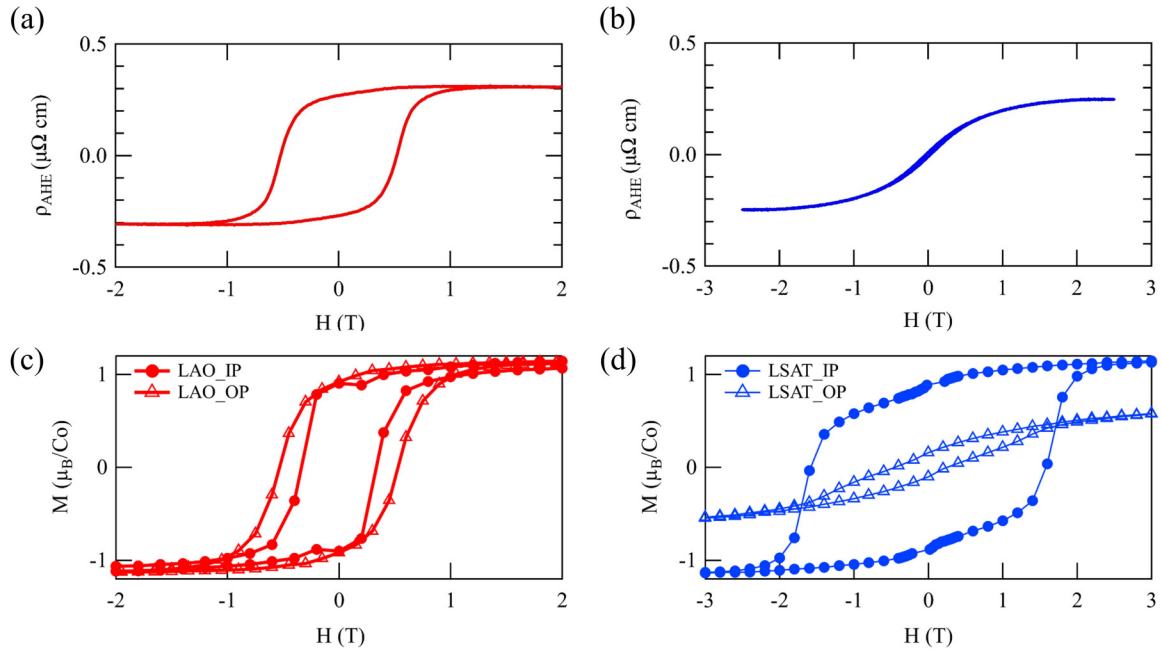

FIG. 3. Magnetic-field dependence of the anomalous Hall resistivity ρ_{AHE} (top) and magnetization M (bottom) of LSCO films on (a), (c) LAO and (b), (d) LSAT substrates. For magnetization measurements, a magnetic field of 5 T was applied in directions parallel and perpendicular to the sample during the cooling process and measurement. All data in (a)–(d) were taken at 20 K.

Pauw method. Both films exhibit metallic conduction down to low temperatures and undergo ferromagnetic transitions as indicated by the hump in the ρ_{xx}-T curves in Figs. 2(a) and 2(b). We note that the ρ_{xx} and the ferromagnetic transition temperature Tc are strain dependent. The film on LAO has a lower ρ_{xx} and a higher Tc than the film on LSAT. The strain-dependent ferromagnetic transitions are also seen from the temperature dependence of the out-of-plane (OP) and in-plane (IP) magnetization in Figs. 2(c) and 2(d). The M-T data were taken under a 1-kOe magnetic field during warming from 5 K after field cooling (FC). The spontaneous magnetization of the compressively strained film is found to develop at ∼220 K while that of the tensilely strained film is seen below 200 K, indicating that the Tc of the compressively strained film is ∼20 K higher than that of the tensilely strained film. The observed change in Tc is in agreement with the previous reports on strain effects on magnetic properties of LSCO films [27,28]. These observations indicate that the compressive strain and the resultant shrinkage in the in-plane lattice constant enhance the itinerancy of the conduction carriers, resulting in the lower resistivity, and increase ferromagnetic exchange interactions [27], making the ferromagnetic state of LSCO more stable. Another important observation in Figs. 2(c) and 2(d) is that the magnitudes of the OP and IP magnetization strongly depend on the type of strain (compressive or tensile). This implies the substrate-induced strain and resultant structural distortions influence the magnetic anisotropy of LSCO. The magnitudes of the OP and IP magnetization of the compressively strained film are about the same, implying the magnetization also has an OP component. On the other hand, the IP magnetization of the tensilely strained film is much larger than the OP one, indicating that in-plane magnetic anisotropy is stabilized.

To further evaluate the magnetic anisotropy and magnetic easy-axis directions of the compressively and tensilely strained films, we measured magnetic-field dependence of the Hall resistivity and OP and IP magnetization at 20 K, as seen in Figs. 3(a) and 3(b). The anomalous part of the Hall resistivity, ρ_{AHE}, as a function of the magnetic field reveals distinct magnetic anisotropy between the films. The ρ_{AHE} was extracted by antisymmetrizing the Hall resistivity and then subtracting the normal part from the antisymmetrized resistivity. The normal parts of the Hall resistivity of both films are found to be positive and on the order of $0.1-0.01\,\mu\,\Omega$ cm at 1 T, and the carrier concentration calculated from the normal part is around $10^{21}-10^{22}\,\mathrm{cm}^{-3}$ at 20 K. The ρ_{AHE} of the compressively strained film shows a large hysteresis against the field sweeping directions, revealing the existence of the perpendicular component of the magnetization. On the other hand, the ρ_{AHE} of the tensilely strained film shows no hysteresis and this is a characteristic of in-plane magnetization. The magnetic-field dependence of the OP and IP magnetic moments at 20 K of the compressively and tensilely strained films are shown in Figs. 3(c) and 3(d), respectively. For the compressively strained LSCO, the hysteretic behaviors of OP and IP magnetization are about the same. In addition, both saturated moment (∼1.1μ_B/Co) and coercive fields (∼5000 Oe) are comparable between the OP and IP loops. These observations indicate that the magnetization for the compressively strained LSCO is tilted with respect to the out-of-plane direction, possessing both in-plane and out-of-plane components of magnetization. The magnetic easy axis probably points in the diagonal directions (45° from the out-of-plane direction). On the other hand, the behavior of the magnetization loops for the tensilely strained film [Fig. 3(d)] is distinct from that of the loops for the compressively strained film. The

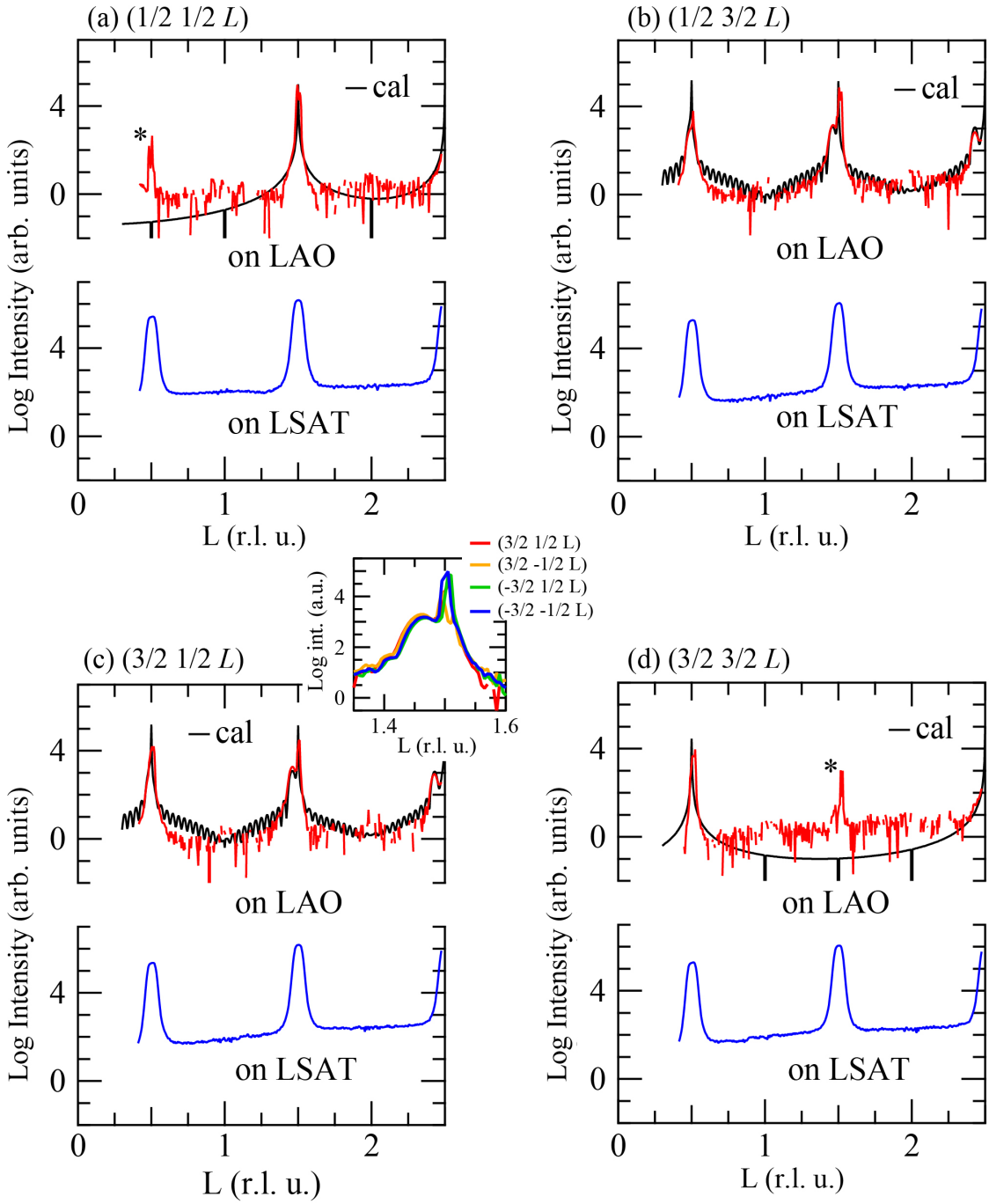

FIG. 4. $(1/2\,1/2\,L)$, $(1/2\,3/2\,L)$, $(3/2\,1/2\,L)$, and $(3/2\,3/2\,L)$ profiles for the compressively and tensilely strained LSCO films (on the LAO and LSAT substrates). The black lines are profiles calculated by the optimized model of the LSCO/LAO. The peaks marked with the asterisk (*) in the profiles are originally forbidden but appear with weak intensity probably due to multiple scatterings in the substrate. The inset shows the profiles around the $(3/2\,1/2\,3/2)$, $(-3/2\,1/2\,3/2)$, $(3/2\,-1/2\,3/2)$, and $(-3/2\,-1/2\,3/2)$ reflections. In the profiles for the tensilely strained film, relatively high background signal from the LSAT substrate were observed, which hinder quantitative analysis on half-order reflection intensities.

IP magnetization shows a larger hysteresis loop with the saturated moment as large as 1.1 μ_B/Co, while the hysteresis behavior for the OP magnetization is strongly suppressed. The observed behavior is in good agreement with what is expected from magnetic films having the in-plane magnetic anisotropy and is consistent with the M-T results [Fig. 2(d)]. It should be also pointed out that the saturated magnetic moments for both films are almost the same ($\sim$1.1μ_B/Co). These observations indicate that the types of the epitaxial strain and its resultant modifications in the CoO_6 octahedral distortions strongly influence the magnetic anisotropy while the valence and spin states of the Co ion in LSCO are less influenced.

To delineate how the CoO_6 octahedral distortions are linked to the observed strain-dependent properties, we carried

TABLE I. Structural parameters for the 10-nm-thick LSCO films on the LAO and LSAT substrates. The parameters were determined from the synchrotron x-ray-diffraction profiles and their analysis based on the model calculations. Note that the films are coherently grown on both substrates and the in-plane lattice constants of the films are identical to those of the substrates.

	Co–O bond length	Co–O–Co bond angle	Rotation pattern	Rotation angle
LSCO film (on LAO sub.)	$d_{\text{out}} = 1.949$ Å $d_{\text{in}} = 1.897$ Å	$\theta_{\text{out}} = 180^\circ$ $\theta_{\text{in}} = 175^\circ$	$a^0a^0c^-$	$\alpha_{\text{rot}} = 0^\circ$ $\beta_{\text{rot}} = 0^\circ$ $\gamma_{\text{rot}} = 2.5^\circ \pm 0.2^\circ$
LSCO film (on LSAT sub.)	$d_{\text{out}} = 1.897$ Å $d_{\text{in}} = 1.934$ Å	$\theta_{\text{out}} = \theta_{\text{in}} = 180^\circ$	$a^0a^0a^0$	$\alpha_{\text{rot}} = \beta_{\text{rot}} = \gamma_{\text{rot}} = 0^\circ$
Bulk LSCO	$d_{\text{out}} = d_{\text{in}} = 1.920$ Å	$\theta_{\text{out}} = \theta_{\text{in}} = 175.5^\circ$	$a^-a^-a^-$	$\beta_{\text{rot}} = \beta_{\text{rot}} = \gamma_{\text{rot}} \sim 1.6^\circ$

out synchrotron x-ray-diffraction measurements at the BL13XU beamline [29] in SPring-8 and quantitatively evaluated octahedral distortions accommodated in the compressively and tensilely strained films. Details of the measurements were provided in our previous reports [30,31]. Note that the observed diffraction intensity was corrected by the factors based on the footprint, the polarization of the incident beam (20 keV), and the Lorentz factor. The reciprocal lattice units used in our profiles are based on the pseudocubic perovskite lattice constants of the substrates. Figure 4 shows the $(1/2\,1/2\,L)$, $(1/2\,3/2\,L)$, $(3/2\,1/2\,L)$, and $(3/2\,3/2\,L)$ profiles for the compressively and tensilely strained films on the LAO and LSAT substrates. We see that while both LAO and LSAT substrates give dominant half-order reflections, only the LSCO film on the LAO substrate exhibits half-order reflections that are characteristic for CoO_6 octahedral rotations. The half-order reflections of the compressively strained film (on the LAO substrate) are seen only when H, K, and L are half integers and $H \neq K$. Reflections seen in the $(1/2\,1/2\,L)$ and $(3/2\,3/2\,L)$ profiles are from the substrates in Figs. 4(a) and 4(d). This indicates that the CoO_6 octahedra deformed under the substrate-induced compressive strain have the out-of-phase rotations about the out-of-plane direction, while there are no rotations about the in-plane directions. The rotation pattern in the compressively strained film can be described as $a^0a^0c^-$ in the Glazer notation. On the other hand, the tensilely strained film (on the LSAT substrate) exhibits no half-order reflections and thus accommodates no CoO_6 rotations, indicating that the rotation pattern is described as $a^0a^0a^0$, which agrees with the previous report [32]. It is therefore only the substrate-induced tensile strain that results in the deformations in the CoO_6 octahedra. Structural parameters for the deformed CoO_6 octahedra under the compressive and tensile strains are provided in Table I. It should be also noted that oxygen vacancy orderings in LSCO [33–36] might affect oxygen octahedral distortions. However, no superstructure reflections that could be ascribed to such vacancy orderings are seen in our films.

We also built structural models of LSCO/LAO and reproduced the observed half-order Bragg intensity so as to quantitatively evaluate the Co–O bond lengths and the Co–O–Co bond angles. It should be noted that because LAO has the rhombohedral structure, the (001)-oriented substrate includes four crystallographic domains that are defined by relative rotation directions (positive or negative in the rotation angles) for the AlO_6 octahedron at the origin, and thus has different structural factors. Given that octahedral rotations in the substrate are propagated through the heterointerface to some degree, the crystallographic domains in the substrate induce formation of crystallographic domains in the LSCO layer whose octahedral rotation patterns are identical, but whose structural factors differ between domains. As shown in the inset of Fig. 4, the variations of the intensities of the $(3/2\,1/2\,3/2)$, $(-3/2\,1/2\,3/2)$, $(3/2\,-1/2\,3/2)$ and $(-3/2\,-1/2\,3/2)$ reflections from the films are rather small, about 15% in the average intensity of these four reflections. Thus, these domains in our LSCO/LAO model are assumed to be equally distributed. The structural parameters, including the bond lengths and angles, are summarized in Table I. Profiles calculated with our optimized model are included (the black lines) in Fig. 4, reasonably reproducing the observed half-order reflection intensities. The octahedral rotation angle about the out-of-plane direction (the γ rotation angle) in the film is relatively small, $2.5^\circ \pm 0.2^\circ$, although this obtained angle is slightly larger than that of the bulk because the shrinkage of the in-plane lattice constants resulting from the compressive strain can increase the γ octahedral rotations [24,30]. It should be also pointed out that the in-plane and out-of-plane Co–O bond lengths ($d_{\text{in\_Co–O}}$ and $d_{\text{out\_Co–O}}$) of the compressively strained film are comparable to the $d_{\text{out\_Co–O}}$ and $d_{\text{in\_Co–O}}$ of the tensilely strained film. The observed strain-induced changes in the Co–O bond lengths are qualitatively in agreement with the previous investigation of the bond lengths by extended x-ray-absorption fine structure [28]. The strain-induced changes in the bond lengths and angles are known to modify energy levels of the t_{2g} and e_g bands, influencing films' properties. While the bond angles are closely related to the bandwidth, the deviation in the Co–O–Co bond angle of the compressively strained film is only 6° from 180°, implying negligibly small influence of the bond angle on electronic configurations in the Co ions in the film. On the other hand, changes in the bond length play key roles in the strain-dependent properties of the films through modified hybridization between Co *3d* and O *2p* orbitals. For the compressively strained film, the shrinkage of the in-plane bond length promotes orbital overlaps between Co and O, and lower energy levels of the d_{yz} and d_{zx} bands, resulting in larger bandwidth and ferromagnetic exchange coupling [27,28], consequently leading to lower electrical resistivity and increased ferromagnetic transition temperature.

Furthermore, the d_{yz} and d_{zx} bands are doubly degenerated and can be mixed, exhibiting the perpendicular orbital moment, resulting in perpendicular magnetic anisotropy through spin-orbit interaction. On the other hand, the expansion of in-plane bond length causes suppression of the orbital overlaps, leading to lower energy levels of the d_{xy} orbitals, which is responsible for the observation of higher electrical resistivity and decreased ferromagnetic transition temperature. We note for the tensilely strained film that the strain-induced change in the bond length would not lead to the d_{yz}/d_{zx} orbital mixings, which explains the observation of in-plane magnetic anisotropy.

IV. SUMMARY

We show the close link between the CoO_6 oxygen octahedral distortions, and magnetic and transport properties in LSCO films. The electrical resistivity and ferromagnetic transition temperature of LSCO are found to be closely associated with the strain-induced changes in the Co–O bond lengths that result in modulations of the Co–O orbital hybridization. Furthermore, the octahedral distortions are found to influence magnetic anisotropy. The perpendicular magnetic anisotropy is stabilized under the compressive strain that leads to the out-of-plane orbital magnetic moment through the strain-induced modifications in the t_{2g} orbital mixings. Our results highlight the significance of oxygen octahedral distortions in determining and controlling structure-property relationships of LSCO.

ACKNOWLEDGMENTS

We thank Dr. M. Goto and Dr. M. Patino for useful discussions. This work was partially supported by a grant for the Integrated Research Consortium on Chemical Sciences, by Grants-in-Aid for Scientific Research (Grants No. JP16H02266, No. JP17H05217, No. JP17H04813, and No. JP17F17719), by a JSPS Core-to-Core program (A), by a grant for the Joint Project of Chemical Synthesis Core Research Institutions from the Ministry of Education, Culture, Sports, Science and Technology (MEXT) of Japan, and by Iketani Science and Technology Foundation. The measurements at SPring-8 were made with the approval of the Japan Synchrotron Radiation Research Institute (Proposal No. 2018A1273).

[1] D. G. Schlom, L.-Q. Chen, X. Pan, A. Schmehl, and M. A. Zurbuchen, J. Am. Ceram. Soc. **91**, 2429 (2008).
[2] S. A. Chambers, Adv. Mater. **22**, 219 (2010).
[3] P. Zubko, S. Gariglio, M. Gabay, P. Ghosez, and J.-M. Triscone, Annu. Rev. Condens. Matter Phys. **2**, 141 (2011).
[4] J. M. Rondinelli, S. J. May, and J. W. Freeland, MRS Bull. **37**, 261 (2012).
[5] C. H. Ahn, K. M. Rabe, and J.-M. Triscone, Science **303**, 488 (2004).
[6] D. G. Schlom, L.-Q. Chen, C.-B. Eom, K. M. Rabe, S. K. Streiffer, and J.-M. Triscone, Annu. Rev. Mater. Res. **37**, 589 (2007).
[7] A. Bhattacharya and S. J. May, Annu. Rev. Mater. Res. **44**, 65 (2014).
[8] Z. Liao, M. Huijben, Z. Zhong, N. Gauquelin, S. Macke, R. J. Green, S. Van Aert, J. Verbeeck, G. Van Tendeloo, K. Held, G. A. Sawatzky, G. Koster, and G. Rijnders, Nat. Mater. **15**, 425 (2016).
[9] A. Y. Borisevich, H. J. Chang, M. Huijben, M. P. Oxley, S. Okamoto, M. K. Niranjan, J. D. Burton, E. Y. Tsymbal, Y. H. Chu, P. Yu, R. Ramesh, S. V. Kalinin, and S. J. Pennycook, Phys. Rev. Lett. **105**, 087204 (2010).
[10] J. M. Rondinelli and N. A. Spaldin, Adv. Mater. **23**, 3363 (2011).
[11] E. J. Moon, Q. He, S. Ghosh, B. J. Kirby, S. T. Pantelides, A. Y. Borisevich, and S. J. May, Phys. Rev. Lett. **119**, 197204 (2017).
[12] D. Kan, R. Aso, R. Sato, M. Haruta, H. Kurata, and Y. Shimakawa, Nat. Mater. **15**, 432 (2016).
[13] A. Vailionis, H. Boschker, W. Siemons, E. P. Houwman, D. H. A. Blank, G. Rijnders, and G. Koster, Phys. Rev. B **83**, 064101 (2011).
[14] A. M. Glazer, Acta Crystallogr., Sect. B **28**, 3384 (1972).
[15] V. G. Sathe, A. V. Pimpale, V. Siruguri, and S. K. Paranjpe, J. Phys.: Condens. Matter **8**, 3889 (1996).
[16] A. Mineshige, M. Inaba, T. Yao, Z. Ogumi, K. Kikuchi, and M. Kawase, J. Solid State Chem. **121**, 423 (1996).
[17] M. A. Señarís-Rodríguez and J. B. Goodenough, J. Solid State Chem. **118**, 323 (1995).
[18] A. Senchuk, H. P. Kunkel, R. M. Roshko, C. Viddal, L. Wei, G. Williams, and X. Z. Zhou, Eur. Phys. J. B **37**, 285 (2004).
[19] E.-J. Guo, R. D. Desautels, D. Keavney, A. Herklotz, T. Z. Ward, M. R. Fitzsimmons, and H. N. Lee, Phys. Rev. Mater. **3**, 014407 (2019).
[20] D. Fuchs, C. Pinta, T. Schwarz, P. Schweiss, P. Nagel, S. Schuppler, R. Schneider, M. Merz, G. Roth, and H. v. Löhneysen, Phys. Rev. B **75**, 144402 (2007).
[21] L. Qiao, J. H. Jang, D. J. Singh, Z. Gai, H. Xiao, A. Mehta, R. K. Vasudevan, A. Tselev, Z. Feng, H. Zhou, S. Li, W. Prellier, X. Zu, Z. Liu, A. Borisevich, A. P. Baddorf, and M. D. Biegalski, Nano Lett. **15**, 4677 (2015).
[22] J. Fujioka, Y. Yamasaki, H. Nakao, R. Kumai, Y. Murakami, M. Nakamura, M. Kawasaki, and Y. Tokura, Phys. Rev. Lett. **111**, 027206 (2013).
[23] N. Sundaram, Y. Jiang, I. E. Anderson, D. P. Belanger, C. H. Booth, F. Bridges, J. F. Mitchell, T. Proffen, and H. Zheng, Phys. Rev. Lett. **102**, 026401 (2009).
[24] S. J. May, J. W. Kim, J. M. Rondinelli, E. Karapetrova, N. A. Spaldin, A. Bhattacharya, and P. J. Ryan, Phys. Rev. B **82**, 014110 (2010).
[25] R. Aso, D. Kan, Y. Shimakawa, and H. Kurata, Sci. Rep. **3**, 2214 (2013).
[26] T. T. Fister, H. Zhou, Z. Luo, S. S. A. Seo, S. O. Hruszkewycz, D. L. Proffit, J. A. Eastman, P. H. Fuoss, P. M. Baldo, H. N. Lee, and D. D. Fong, APL Mater. **2**, 021102 (2014).
[27] C. Xie, J. I. Budnick, B. O. Wells, and J. C. Woicik, Appl. Phys. Lett. **91**, 172509 (2007).

[28] C. K. Xie, J. I. Budnick, W. A. Hines, B. O. Wells, and J. C. Woicik, Appl. Phys. Lett. **93**, 182507 (2008).

[29] O. Sakata, Y. Furukawa, S. Goto, T. Mochizuki, T. Uruga, K. Takeshita, H. Ohashi, T. Ohata, T. Matsushita, S. Takahashi, H. Tajiri, T. Ishikawa, M. Nakamura, M. Ito, K. Sumitani, T. Takahashi, T. Shimura, A. Saito, and M. Takahasi, Surf. Rev. Lett. **10**, 543 (2003).

[30] D. Kan, M. Anada, Y. Wakabayashi, H. Tajiri, and Y. Shimakawa, J. Appl. Phys. **123**, 235303 (2018).

[31] D. Kan, Y. Wakabayashi, H. Tajiri, and Y. Shimakawa, Phys. Rev. B **94**, 024112 (2016).

[32] M. D. Biegalski, Y. Takamura, A. Mehta, Z. Gai, S. V. Kalinin, H. Ambaye, V. Lauter, D. Fong, S. T. Pantelides, Y. M. Kim, J. He, A. Borisevich, W. Siemons, and H. M. Christen, Adv. Mater. Interfaces **1**, 1400203 (2014).

[33] Y.-M. Kim, J. He, M. D. Biegalski, H. Ambaye, V. Lauter, H. M. Christen, S. T. Pantelides, S. J. Pennycook, S. V. Kalinin, and A. Y. Borisevich, Nat. Mater. **11**, 888 (2012).

[34] J. Walter, S. Bose, M. Cabero, G. Yu, M. Greven, M. Varela, and C. Leighton, Phys. Rev. Mater. **2**, 111404 (2018).

[35] W. S. Choi, J.-H. Kwon, H. Jeen, J. E. Hamann-Borrero, A. Radi, S. Macke, R. Sutarto, F. He, G. A. Sawatzky, V. Hinkov, M. Kim, and H. N. Lee, Nano Lett. **12**, 4966 (2012).

[36] J. Gazquez, S. Bose, M. Sharma, M. A. Torija, S. J. Pennycook, C. Leighton, and M. Varela, APL Mater. **1**, 012105 (2013).